Icarus 299 (2018) 364–369

Contents lists available at ScienceDirect

Icarus

journal homepage: www.elsevier.com/locate/icarus

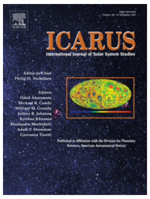

Low probability of tropical cyclones on ocean planets in the habitable zones of M dwarfs

Jiayu Bin[a], Feng Tian[a,*], Yanluan Lin[a], Yuwei Wang[b]

[a] Ministry of Education Key Laboratory for Earth System Modeling, Center for Earth System Science, Tsinghua University, Beijing 100084, China
[b] Department of Atmospheric and Oceanic Sciences, McGill University, Montreal, Quebec H3A 0B9, Canada

ARTICLE INFO

Article history:
Received 2 December 2016
Revised 23 July 2017
Accepted 7 August 2017
Available online 18 August 2017

Keywords:
Exoplanets
Tropical cyclones

ABSTRACT

The genesis potential index (GPI) of tropical cyclones (TC) on ocean planets in the habitable zones of M dwarfs is analyzed based on 3D GCM simulations. We found that GPI on these planets are smaller than those in TC basins on the Earth mainly because of slow rotation of such planets. GPI's on exoplanets with eccentric orbits are strong function of time with values generally greater than those on circular orbits. Future high resolution models are needed to better understand whether TCs could form on ocean exoplanets, and what their potential intensities and distributions might be.

1. Introduction

Most studies on the climate of rocky exoplanets focus on large-scale atmospheric circulation patterns (Pierrehumbert, 2010; Yang et al., 2013; Hu and Yang, 2014; Wang et al., 2014, 2016; Wolf and Toon, 2015; Kopparapu et al., 2016). On the Earth the distribution of life is influenced by meteorological phenomena. Tropical cyclones (TC), one of the most destructive weather on the Earth, induce heavy precipitation, strong winds, and storm surges (Rappaport, 2000). On the other hand, TC can cause upwelling of nutrient-rich water from deep ocean, which supplies the growth of phytoplankton (Shibano et al., 2011). Thus it is useful to study the frequency and distribution of TC on potentially habitable exoplanets.

Gray (1979) developed an index to describe the seasonal and spatial variability of observed TC, which includes parameters specific to modern climate of the Earth. Inspired by Gray's work, Emanuel and Nolan (2004) developed a more general genesis potential index (GPI). Based on monthly NCEP Reanalysis data from 1950 to 2005 (Kalnay et al., 1996), GPI calculated between 60°S and 60°N (Camago et al., 2007) are in good agreement with observed spatial distribution and seasonal variation of tropical cyclones. In addition, the properties of TC on the Earth in the past and future climate can be projected using general circulation models (GCMs) (Knuston et al., 2010; Lin et al., 2015; Yan et al., 2016).

Although applying a cyclone genesis index developed for the Earth to exoplanets may not reflect realistic cyclone activities on exoplanets, exoplanet climate might be influenced by cyclones through modifications of ocean heat transport (Emanuel, 2001; Jansen et al., 2010). Thus, a theoretical analysis of cyclone genesis could be helpful to better understand exoplanet climate. In this work we apply the GPI analysis to evaluate the probability of TC on ocean exoplanets in the HZ of M dwarfs based on GCM results.

2. Methods

2.1. Evaluation of TC genesis

According to Emanuel and Nolan (2004),

$$\mathrm{GPI} = \left|10^5\eta\right|^{3/2}\left(\frac{H}{50}\right)^3\left(\frac{V_{\mathrm{pot}}}{70}\right)^3(1\;+\;0.1V_{\mathrm{shear}})^{-2} \tag{1}$$

where η is the absolute vorticity (s^{-1}) at 850 hPa (in this work we use its vertical component), H is the relative humidity at 600 hPa (%), V_{shear} is the vertical wind shear (m/s) between 850 and 200 hPa, and V_{pot} is the potential intensity (m/s), a measure of the maximum surface wind which can be sustained by a TC within a certain environment. V_{pot} can be calculated based on sea surface temperature (SST), sea level pressure, and the vertical profiles of temperature and specific humidity (Bister and Emanuel, 2002a).

$$V_{\mathrm{pot}}^2 = \frac{C_k}{C_D}\frac{SST}{T_o}(CAPE_{ms} - CAPE_m) \tag{2}$$

where C_k and C_D are the exchange coefficients for enthalpy and the drag coefficient, respectively. Because the surface conditions on exoplanets in this study are similar to those on the Earth, we use $\frac{C_k}{C_D} = 0.9$, which is the typical value for Earth's TC. T_o is the mean

---

* Corresponding author.
E-mail address: tianfengco@mail.tsinghua.edu.cn (F. Tian).

http://dx.doi.org/10.1016/j.icarus.2017.08.007

temperature at the outflow level. $\frac{SST}{T_o}$ represents the effect of dissipative heating. $CAPE_m$ is the convective available potential energy (CAPE) of an air parcel in boundary layer evaluated at the radius of maximum wind. $CAPE_{ms}$ is the CAPE of the same air parcel if it is in equilibrium with sea surface and saturated. The difference between $CAPE_{ms}$ and $CAPE_m$ indicates the thermodynamic disequilibrium between the unsaturated air parcel and the sea surface, which determines how much energy a TC can uptake from the sea surface. Typically a lower T_o in combination with the same SST means a higher thermodynamic efficiency of classic Carnot heat engine of the cyclone system (Emanuel, 1986). In Emanuel (1994),

$$CAPE = \int_{p_t}^{p_b} R_d (T_{vp} - T_{ve}) d\ln p \tag{3}$$

where p_b and p_t are the pressures at the lowest level of the environment profile and the level of neutral buoyancy (LNB) of the air parcel, respectively. For simplicity the LNB is taken as the outflow level. T_{vp} and T_{ve} are the virtual temperature of an air parcel and that of the environment, respectively. T_v can be calculated based on temperature T and water vapor mixing ratio r.

$$T_v = T\frac{1 + r/\epsilon}{1 + r} \tag{4}$$

where $\epsilon = \frac{R_d}{R_v} \approx 0.622$, R_d and R_v are gas constants of dry air and water vapor, respectively. When computing $CAPE_{ms}$ and $CAPE_m$, the virtual temperatures of the air parcels are T_{vpms} and T_{vpm}, respectively.

2.2. Results of GCM simulations

The liquid water habitable zone (HZ) is at ~0.1 AU around M dwarfs because of low stellar luminosities (Kasting et al., 1993). At this distance, planets are most likely to be synchronously rotating (rotation–orbit period ratio $p = 1$), with a limited open ocean existing around the substellar point (an eyeball pattern, Pierrehumbert, 2010). Inputs for the GPI analysis in this work are based on GCM simulations using the Community Atmosphere Model version 3 (Collins et al., 2004) with slab ocean (without ocean heat flux), thermodynamic sea ice, and 128 × 64 grids. The slab ocean has a uniform depth of 50 m, which is the same as the average depth of mixing layer on the Earth and is commonly used in previous GCM for exoplanet climate studies (Yang et al., 2013; Yang et al., 2014; Wang et al., 2016; Kopparaku et al., 2016). The planets are assumed to be ocean planets, with zero obliquities and orbital periods of 28 days, and with atmospheres containing 1 bar N_2, 355 ppmv CO_2 and no ozone. Orbit eccentricities 0.4 (case 1) and 0 (case 2) are used in the GCM simulations. In case 1 the incident stellar radiation at the top of the planet's atmosphere (TOA) is set to 1237 W/m^2 (the value in case 2) when the planet-star distance is equal to the orbit's semi-major axis. In case 1, the planet is assumed to be at periastron on day 1 with a substellar longitude of 180°. After the simulation reaches the steady state, 10 exoplanet years of GCM data are used to produce daily mean outputs, which are then used in the GPI analysis.

Fig. 1a and b shows the annual mean SST distributions in both cases. As shown previously (Pierrehumbert, 2010; Wang et al., 2014), the warm region (>290 K) locates near the substellar point, while the minimum SST (~200 K) locates in high latitude regions and the far sides of the planets. The area with high SST is larger in case 1 ($e = 0.4$) than that in case 2 ($e = 0$) because the substeller point stays at 180° in case 2 but migrates around 180° longitude in case 1. In addition the orbital averaged incident stellar radiation in case 1 is greater (~1346 W/m^2) than that in case 2. Thus the global mean and maximum surface temperature in case 1 are both higher than those in case 2. These climate patterns are typical in habitable zone exoplanet GCM simulations (Pierrehumbert, 2010; Wang et al., 2014, 2016).

The 3-D wind fields at 850 hPa pressure level (Fig. 1c and d) show a large-scale convergence pattern for the horizontal winds and a ring-shape pattern for vertical winds on the near side of the planet. The climatological wind patterns are produced by a slowly moving substeller point ($e = 0.4$, case 1) or a fixed substellar point ($e = 0$, case 2), in which cases a region with continuous and symmetric heating exist. This scenario is similar to the solution for symmetric heating about the Earth's equator in the Gill Model (Gill, 1980), but with a much larger heating area. In the Gill model, the localized heating confined within 10° of the Equator generates Rossby waves that creates westerlies and cyclonic flows on the west margins of the heating zone, and Kelvin wave that creates easterlies in the region. In both cases 1 and 2, cyclonic flows can be found to the west of the subtellar region, but with much larger scale and extending to higher latitude in comparison to those in the Gill model.

3. Results and discussions

The distributions of maximum GPI in both cases are shown in Fig. 2. The white areas have SST <5 °C (Fig. 1). TC does not occur in cold regions on the Earth and thus there is no calculation at these locations. The zonal symmetry reflects the zero obliquity assumption in the GCM simulations. The regions with high GPI in Fig. 2 indicate the locations with highest possibility of TC genesis, in analog to TC basins on the Earth. The maximum GPI in case 1 is ~6 in regions near 180° longitude (Fig. 2a). The maximum GPI in case 2 is ~10 times smaller than that in case 1 (Fig. 2b).

According to (1), small wind shear, high relative humidity, high absolute vorticity, and high potential intensity all lead to greater GPI. The mean (average over 20 exoplanet years) values of these variables in the analyzed region show that the potential intensity is the most important variable contributing to the greater GPI on day 20 (Table 1, part I).

Fig. 3a shows that the mean GPI in the region (30°S-30°N and 120°E-120°W) in case 1 is a strong function of time, with a peak value of ~0.27 on day 20 when the planet is approaching the periastron (the substellar point ~140°E). The GPI in case 2 is constant in time and more than 20 times smaller than the peak value in case 1 (Fig. 3a). M dwarfs' habitable zone planets on circular orbits have rather small potential of TC genesis, while those on eccentric orbits may have higher potential.

The temporal variations of regional mean GPI also follow the trend of regional mean potential intensity Fig. 3b). Table 1 (part II) shows that the mean $CAPE_m$ is negligible in comparison with $CAPE_{ms}$ in the evaluated region. Thus the potential intensity is approximately proportional to $\sqrt{\frac{SST}{T_o}}$ and $\sqrt{CAPE_{ms}}$ according to (2). $CAPE_{ms}$ measures how much energy an air parcel can uptake from the sea when ascending in the environment if it is saturated at sea surface temperature. The temporal variations of $\frac{SST}{T_o}$ (Fig. 3c) and $CAPE_{ms}$ (Fig. 3d) in the same region correspond well with those of the mean GPI and the potential intensity (Fig. 3a, b). $CAPE_{ms}$ and $\frac{SST}{T_o}$ in case 2 ($e = 0$) are both significantly smaller than those in case 1 ($e = 0.4$), indicating much weaker energy uptake potential and dissipative heating on a $e = 0$ planet.

Fig. 4a and b shows the mean profiles of virtual temperature used to calculate $CAPE_{ms}$. In this analysis, the area surrounded by the profiles of T_{vpms} and T_{ve} between LNB (the crossing points of T_{vpms} and T_{ve}) and 900 hPa is proportional to the value of $CAPE_{ms}$. The profiles of T_{vpms} depend largely on SST, which varies little in both cases as a result of the high heat capacity of ocean (Table 1, part II). Thus the differences in $CAPE_{ms}$ and $\frac{SST}{T_o}$ in case 1 are mainly determined by the differences in vertical T_{ve} profiles